Spectroscopic study of ablation and recombination processes in a laser-produced ZnO plasma

S. Namba,[a] R. Nozu, and K. Takiyama
Graduate School of Engineering, Hiroshima University, Kagamiyama 1-4-1, Higashi-Hiroshima, Hiroshima 739-8527, Japan

T. Oda
Department of Bio-Recycling, Faculty of Engineering, Hiroshima Kokusai Gakuin University, 6-20-1 Nakano Aki-ku, Hiroshima 739-0321, Japan

(Received 28 April 2005; accepted 1 March 2006; published online 6 April 2006)

Characteristics of laser-produced ZnO plasmas have been investigated by spectroscopic observations. In particular, the ablation dynamics and recombination process in vacuum or gas atmospheres (helium or oxygen) were studied on the basis of atomic physics. During and immediately after a laser irradiation, plasma parameters, such as electron temperature and electron density, were deduced from continuum and line spectra. In addition, the expansion velocities of ions and atoms were determined by time-of-flight transients of the emission spectra. As for the neutralization process of the expanding plasmas in vacuum, it was found that the radiative recombination dominated the plasma neutralization process. On the other hand, long-lived bright emissions that had a roughly spherical shape were observed in a helium atmosphere. This can be explained by the scattering of particles ejected from the target and rapid plasma cooling due to the collision with an ambient gas. Thus, the three-body recombination responsible for the intense emissions played an important role for electron-ion recombination. Moreover, it was found that a charge exchange recombination between He^+ and Zn occurred near the target surface in helium. Although similar results were obtained in an oxygen atmosphere, the peak intensities were much higher than those in helium, implying that the additional cooling associated with the inherent properties of molecules may significantly influence the plasma neutralization. © *2006 American Institute of Physics*. [DOI: 10.1063/1.2190715]

I. INTRODUCTION

Laser ablation plasmas have been extensively studied for the fabrication of various high-quality thin films. For example, ZnO thin films, which are regarded as promising candidates for ultraviolet laser diodes,[1,2] can be grown by pulsed laser deposition (PLD). In this process, the plasma is usually produced in a gas atmosphere, where gas species and their relative pressures are thought to play important roles in film growth. For example, silicon nanoparticles were observed to form in a laser-produced Si plasma under an argon atmosphere.[3] Recently, a ZnO nanorod that exhibited good nano-optical properties was fabricated on a sapphire substrate under an oxygen atmosphere.[4] Thus, the effects of the type and pressure of the gas species on the deposition rate and quality of the thin film need to be clarified.

A deeper understanding of the atomic processes involved in laser plasmas is essential for thin film deposition applications since these processes strongly influence the deposition efficiency on the substrate. For instance, a shock front in the ablation plume was observed in a gas atmosphere, where the plasma particles lost their initial momentum due to collision with the ambient gas.[5] As a result, recombination occurred more quickly than in vacuum. Since the plasma cooling induced by the contact dramatically changes the recombination process, this method may provide desirable conditions for the neutralization of laser plasmas, which is essential for depositing neutral atoms on a substrate. Moreover, the interaction with the ambient gas may help to prevent high-energy particles damaging the substrate. Although numerous experiments have been conducted on the applications of thin film growth in various gas atmospheres, the recombination process has not yet been fully understood.

On the other hand, it was found that the molecular activated recombination (MAR) associated with inherent properties of molecules drastically affected the recombination process in divertor plasmas of magnetically confined nuclear fusion devices.[6] As the cross section of MAR could be larger than those of conventional radiative recombination and three-body (3B) recombination, molecular gases may offer an advantage in terms of the efficient neutralization in PLD. Moreover, in the case of molecules, additional energy loss processes, such as vibrational and rotational excitations, can contribute enormously to the plasma cooling. However, little is known about the elementary molecular processes in PLD.

In the present study, we investigate the characteristics of laser ablation ZnO plasmas under vacuum and gas atmospheres at the atomic level. Our purpose is to reveal the sequence of ablation dynamics from ionization to recombination in laser plasmas by time- and spatial-resolved spectroscopic observations. The target temperature, electron temperature, and density during and immediately after a laser irradiation are described. Also, the expansion velocities of

[a]Electronic mail: namba@hiroshima-u.ac.jp

ions and atoms determined by means of time-of-flight (TOF) transients are presented. Finally, the recombination processes under vacuum and gas atmospheres (helium or oxygen) at various pressures are discussed in detail.

II. EXPERIMENTAL SETUP

The third-harmonic pulses of a Nd:YAG (yttrium aluminum garnet) laser (Spectra Physics, 355 nm wavelength, 5 ns pulse duration) were used to ablate the ZnO target (purity: 99.9%), which was tilted at ~45° with respect to the direction of the incident laser. The laser beam was focused by a lens (f=750 mm), irradiating the target with a spot size of ~0.5 mm ϕ (full width at half maximum of Gaussian beam profile) and a fluence of ~4.5 J/cm^2. The target disk was rotated continuously to provide a fresh target surface. The vacuum chamber containing no additional gas was evacuated down to $\sim 1 \times 10^{-6}$ Torr with a turbo molecular pump and a rotary pump. Oxygen gas can be fed into the vacuum chamber up to 10 Torr. For the ZnO thin film growth, depositions were carried out under an oxygen atmosphere because of the efficient promotion of oxygenation. In order to investigate the effects of the cooling mechanism and the subsequent recombination process without the effects of molecular processes, an additional experiment was performed under a helium atmosphere.

A visible emission was observed perpendicular to the target surface. The light was collected by a lens onto an optical fiber (plane-type bundle fiber with 48 cores), with which the one-dimensional (1D) spatial distribution of the emission was measured. The light transmitted through the fiber was collected by another lens and focused onto the entrance slit of the spectrometer (SPEX TRIAX190, f =190 mm, 1200 grooves/mm). Finally, spatially resolved spectra were measured by a charge coupled devide (CCD) camera with a gated image intensifier (Princeton Instruments, Inc. I-MAX). The resolution of the optical system was around 0.36 nm. In this study, the CCD camera accumulated 50 shots for improving the signal-to-noise ratio. The spectral sensitivity of the whole optical system was calibrated by a standard tungsten ribbon lamp.

III. RESULTS AND DISCUSSION

A. Continuum spectra during laser irradiation

Figure 1 shows the spatially resolved spectra obtained during and immediately after the laser irradiation. The gate delays from the onset of the laser pulse were set to (a) t=0 and (b) 80 ns, with a gate width of 20 ns. The horizontal and vertical axes correspond to the wavelength (475±23 nm) and spatial position, respectively. There appeared three Zn atomic lines at 468.0 nm ($4\,^3P_0$-$5\,^3S_1$), 472.2 nm ($4\,^3P_1$ -$5\,^3S_1$), and 481.1 nm ($4\,^3P_2$-$5\,^3S_1$) and two Zn^+ ion lines at 491.2 nm ($4\,^2D_{3/2}$-$4\,^2F_{5/2}$) and 492.4 nm ($4\,^2D_{5/2}$-$4\,^2F_{7/2}$) in this wavelength window. As clearly seen, the prominent continuum spectra on the target surface were observed at a delay of t=0. Subsequently, the continuum emission disappeared, and intense atomic and ionic spectra became predominant [Fig. 1(b)].

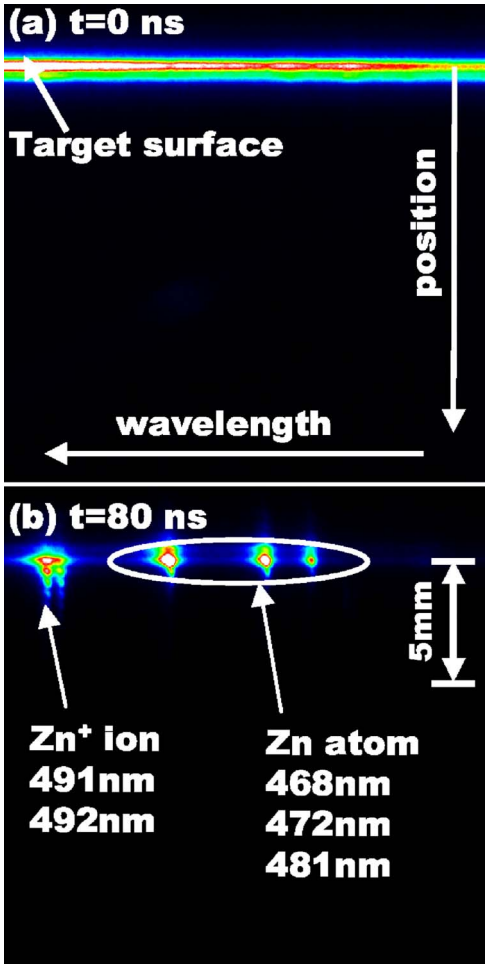

FIG. 1. (Color online) Time- and spatial-resolved spectra of Zn atoms and Zn^+ ions at a delay of t=0 ns (a) and t=80 ns (b) in vacuum. Horizontal and longitudinal axes correspond to the wavelength and spatial position, respectively.

In order to determine the origin of the continuum emission observed, we plotted the calibrated emission coefficient from 430 to 740 nm at a delay of t=0, as shown in Fig. 2 with open circles. The continuum spectra showed a clear minimum near 650 nm. The continuum emission presumably emerges as a result of the blackbody radiation from the target surface itself or from the larger particulates ejected and the plasma in accordance with the thermodynamic equilibrium. Here, Planck's law is expressed by[7]

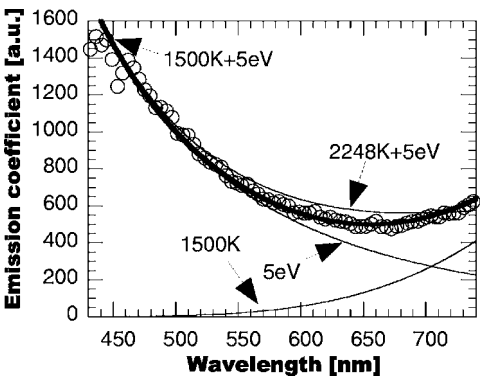

FIG. 2. Continuum spectra observed during and immediately after the laser irradiation (open circles). Planck radiation curves with T=1500 K and 5 eV, as well as T=2248 K and 5 eV, are also shown.

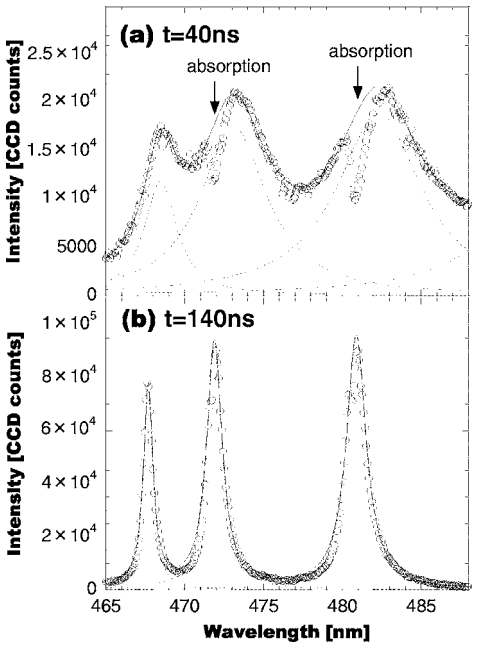

FIG. 3. Stark broadening spectra observed in the vicinity of the target at $t=40$ ns (a) and $t=140$ ns (b). The best Lorentzian fits pertaining to 468.0 nm ($4\,^3P_0$-$5\,^3S_1$), 472.2 nm ($4\,^3P_1$-$5\,^3S_1$), and 481.1 nm ($4\,^3P_2$-$5\,^3S_1$) and their sum are displayed by the dotted and solid curves, respectively. An intense absorption of Zn atoms represented by the arrow was observed at $t=40$ ns.

$$\varepsilon(\lambda)=\frac{8\pi hc}{\lambda^5}\frac{1}{\exp(hc/\lambda kT)-1}, \tag{1}$$

where λ is the wavelength, h the Planck constant, c the velocity of light, k the Boltzmann constant, and T the temperature of the target or the plasma. By using the above equation, the experimental data was fitted for a target temperature of 1500 K and a plasma temperature of 5 eV. A good agreement was obtained between the experimental and calculated results. In Fig. 2, the curve of the target temperature of 2248 K (melting point of ZnO) is also shown for reference. The reason why the target temperature derived from Eq. (1) is much lower than the melting point of ZnO is likely that the area subjected to the laser pulses has a zinc-rich surface (zinc boiling temperature: 1180 K) due to the redeposition of the sputtered zinc from within the ablation plume.[8]

B. Electron density and temperature at the initial stage

Spectra of Zn at the delays of $t=40$ and 140 ns (gate width: 20 ns) at the target surface are shown in Figs. 3(a) and 3(b), respectively. As clearly seen, prominent broadening spectra were observed. From the spectral intensity and profile, the electron temperature and density were determined at different time delays.

First, the electron temperatures T_e of the plasma near the target surface were deduced from the population densities of excited states. Since collisional processes play dominant roles in high-density plasmas, the local thermodynamic equilibrium (LTE) can be established among highly excited levels. Thus, the relationship of population densities of levels i and j is expressed by Boltzmann's law, $n_i/n_j=(g_i/g_j)\exp[-\Delta E/kT_e]$, where n_i and n_j are the population densities of levels i and j, respectively, g is the statistical weight, and ΔE is the energy difference between levels i and j. This assumption is justified for the excited levels because of the high-density plasmas at the early stage. The criterion for the validity of this assumption with respect to the electron temperature and density is described in Ref. 9. In the present study, the population densities of $i=5s\,^3S_1$ and $j=4d\,^3D_3$, which were deduced from the spectral intensities of $4\,^3P_2$-$5\,^3S_1$ and $4\,^3P_2$-$4\,^3D_3$ transitions, respectively, were chosen for the estimation of the electron temperature.

Since the lower levels of these transitions ($4\,^3P_2$) are metastable, however, the intensity around the line center dropped significantly due to self-absorption, as indicated by the arrow in Fig. 3(a). In order to accurately estimate the population densities, therefore, we employed the approximation that the effective transition probability $\Lambda_{ik}A_{ki}$ for the spontaneous transition A_{ki} represents the effect of the self-absorption.[10,11]

If the line profile is assumed to have a Lorentzian profile and the plasma has a cylindrical geometry with a homogeneous distribution, the optical escape factor Λ_{ik} at the column axis ($r=r_0$) for the spectral emission from an upper state k to a lower state i is defined by

$$\Lambda_{ik}(r_0)=\frac{2}{\pi}\int_0^\infty dx\int_0^1 dt\frac{1}{1+x^2}\exp\left(-\frac{\hat{\tau}}{\sqrt{1-t^2}}\frac{1}{1+x^2}\right). \tag{2}$$

Here, $\hat{\tau}$ is the optical depth at the line center, which is given by

$$\hat{\tau}=\frac{e^2}{mc^2}f_{ik}\left[1-\frac{n_k(r_0)}{n_i(r_0)}\frac{g_i}{g_k}\right]\frac{\lambda^2}{\Delta\lambda_L}\int_0^l n_i(\rho)d\rho, \tag{3}$$

where f_{ik} is the absorption oscillator strength, $\Delta\lambda_L$ the Stark width (see below), and l the boundary of the particles. In the present study, the metastable density n_i was determined by the absorption measurement of the $4\,^3P_2$-$5\,^3S_1$ transition, yielding an n_{4p} value of 4×10^{22} m^{-3} at $t=40$ ns. Finally, the electron temperature can be determined by the following equation:

$$\frac{n_{4d}}{n_{5s}}=\frac{I_{4d-4p}/(\Lambda_{4p-4d}A_{4d-4p})}{I_{5s-4p}/(\Lambda_{4p-5s}A_{5s-4p})}=\frac{g_{4d}}{g_{5s}}\exp\left(-\frac{\Delta E}{kT_e}\right), \tag{4}$$

where I is the spectral emissivity observed experimentally. For this transition pair, $\Lambda_{4p-4d}/\Lambda_{4p-5s}\sim0.9$ was obtained at the initial stage. The electron temperature at different time delays is shown in Fig. 4, indicating that the electron temperature was still a few eV even at $t=140$ ns after the laser irradiation.

On the other hand, the best fitted spectra that were deconvoluted by Lorentzian profiles are also shown in Fig. 3 with dotted curves. The fact that the line profiles observed were well reproduced by a Lorentzian shape suggests that the Stark effect in the high-density plasma presumably broadens the spectral profile significantly.[12–14] The electron density n_e, therefore, was determined from the Stark broadening spectra. The linewidths of the $4\,^3P_2$-$5\,^3S_1$ transition estimated from

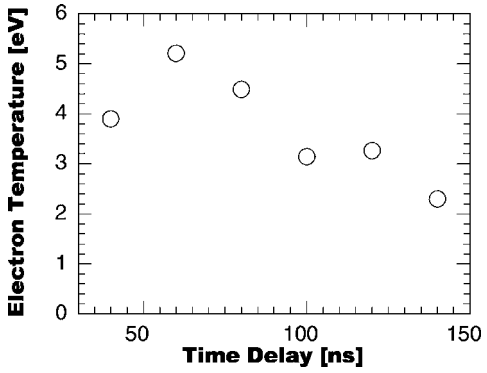

FIG. 4. Electron temperature deduced from Boltzmann's relation between Zn atom 5 $^3S_1$ and 4 $^3D_3$ levels.

the deconvoluted spectra for delays $t=40-140$ ns are listed in Table I. From the broadening widths, electron densities at different time delays were deduced. The spectral broadening width $\Delta\lambda$ consists of three components, namely, resonance $\Delta\lambda_{res}$, van der Waals (vdW) $\Delta\lambda_{vdW}$, and Stark $\Delta\lambda_{Stark}$ broadenings,[15–17]

$$\Delta\lambda = \Delta\lambda_{res} + \Delta\lambda_{vdW} + \Delta\lambda_{Stark}, \tag{5}$$

$$\Delta\lambda_{res} = \frac{\lambda^2}{2\pi c} 2\pi^2 C_3 n_0,$$

$$\Delta\lambda_{vdW} = \frac{\lambda^2}{2\pi c} 8.08 \left(\frac{8kT}{\pi}\right)^{3/10} \sum \left(\frac{1}{\mu_{ij}}\right)^{3/10} C_6 n_j, \tag{6}$$

$$\mu_{ij} = \frac{m_i m_j}{m_i + m_j},$$

$$\Delta\lambda_{Stark} = \frac{\lambda^2}{2\pi c} 11.37 \left(\frac{8kT}{m_e \pi}\right)^{1/6} C_4 n_e,$$

where m_i and m_e are the mass of species i and an electron, respectively, n_0 is the density of the lower level for the relevant radiative transition, n_j is the density of neutral species j, and the other symbols have their usual meanings. The coefficients C_3, C_4, and C_6, which are constants for resonance, Stark, and vdW broadenings, respectively, were reported by Born.[17] For the parameters $n_j=n_e=1\times10^{25}$ m^{-3},

TABLE I. Stark width and shift of the Zn atomic transition 4 $^3P_2$-5 $^3S_1$ (481.1 nm) observed at different time delays after the laser irradiation. The shift estimated by substituting the experimental width into Eq. (7) is shown as well.

Delay (ns)	Stark width $\Delta\lambda$ (nm)	Expt. shift (nm)	Shift from Eq. (7) (nm)
40	6.3	1.7	5.4
60	4.7	1.2	4.0
80	3.8	0.75	3.3
100	2.8	0.5	2.4
120	2.0	0.5	1.7
140	1.5	0.31	1.3

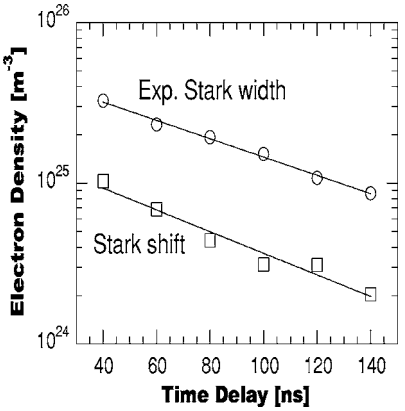

FIG. 5. Electron densities determined from the Stark broadening. Experimental width represents the electron densities that were derived from the Stark widths of the Zn atom 4 $^3P_2$-5 $^3S_1$. The Stark shift shows that the Stark width calculated from experimental Stark shifts was used in determining the electron density.

$n_0=2\times10^{21}$ m^{-3}, and $T=5$ eV, the widths for the 4 $^3P_2$ -5 $^3S_1$ transition are 1.9×10^{-6}, 4.6×10^{-2}, and 2.0 nm for the resonance, vdW, and Stark broadenings, respectively. Thus, the contributions of the resonance and vdW broadenings are negligibly small. The electron density obtained in the vicinity of the target surface is shown in Fig. 5.

Meanwhile, slight wavelength shifts between absorption and emission spectra can also be seen in Fig. 3. It should be noted that the position of the central wavelength of the absorption spectrum did not change. The wavelength shift in the emission spectrum is also listed in Table I. This red shift of the emission spectrum cannot be explained by a Doppler shift. The wavelength shift $\delta\lambda$ due to the vdW and Stark effects is expressed in terms of their broadening widths:[15,17]

$$\delta\lambda = \eta_{vdW}\Delta\lambda_{vdW} + \eta_{Stark}\Delta\lambda_{Stark}. \tag{7}$$

Here, since little data of broadening constants on zinc has been published so far, we employed the ηs derived from the Lindholm-Foley theory, giving $\eta_{vdW}=0.36$ and $\eta_{Stark}=0.86$.[17] Neglecting the contribution of the vdW component, the Stark shifts observed were much smaller than those obtained by substituting the experimental widths into Eq. (7) (see Table I). This discrepancy in the Stark shift is presumably ascribable to the strong self-absorption at the center wavelength in the line profile. Since the lower levels relevant to the 4 $^3P_2$-5 $^3S_1$ transition correspond to the metastable state, we must take into account the influence of radiation trapping to estimate the electron density by measuring the Stark width. Otherwise, the electron density, as well as the Stark width, will be overestimated because of the intensity drop around the central wavelength. This influence is illustrated in Fig. 6, in which both the emission and absorption profiles were assumed to be Lorentzian, and the Stark shift for the emission spectrum was also taken into account. The thick solid and dotted curves represent the spectral profile expected from the experiment and its best fitted Lorentzian curve, respectively. Thus, in the high-density plasma, the Stark width derived from the experimental shift should be used to determine the electron density. The electron densities were also determined by substituting the Stark widths

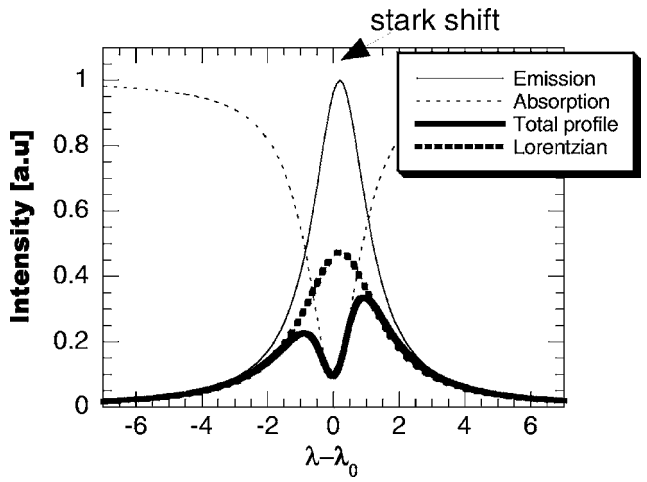

FIG. 6. Distortion of the spectral profile due to radiation trapping. In the central region, both the emission and absorption profiles are assumed to be Lorentzian. The total profile corresponds to the spectrum observed in the experiments. "Lorentzian" represents the best fitted Lorentzian curves of the "total profile." Electron density deduced from the experimental Stark width may be overestimated for optically thick plasmas.

calculated from the measured shifts into Eq. (6) (see Fig. 5). The results showed that the actual densities were much lower than those obtained by the experimental Stark widths.

C. Expansion of plasmas

The expansion velocities of ions and atoms were determined by TOF transients of the spectral emissions. Figure 7(a) shows the spatial distribution of Zn^+ ion spectra ($4\ ^2D_{5/2}$-$4\ ^2F_{7/2}$) at $t=170$, 270, 370 ns (gate width: 20 ns) in vacuum. The fine structures of the spatial distribution were caused by the separation of each core of the bundle fiber. Such temporal evolutions provide a means for estimating the propagation velocities. From the shifts of the peak positions, the expansion velocities of the excited levels of Zn^+ ions were determined to be 1.9×10^4 and 1.7×10^4 m/s for the pairs of 170 and 270 ns and 270 and 370 ns, respectively. The values obtained were in good agreement with the experimental results reported by Girault *et al.*[18] Similarly, the expansion velocity of the atom was evaluated to be $\sim3\times10^3$ m/s.

The difference in velocities between atoms and ions could be explained by the electric field formed near the target.[19,20] At the initial stage, the electrons escape from the target more quickly than ions do. In order to compensate the charge separation, however, the electric field is likely to be formed in front of the target. In addition, the ions are subjected to the Coulombic repulsion by other ions. However, since the atoms expand by an adiabatic free expansion, the velocity is thought to be approximately equal to the sound speed of zinc. The potential derived from the energy difference between ions and atoms corresponds to 2.7×10^2 V.

Meanwhile, the expansion velocity in He at 2.5 Torr was also derived by the TOF method. From Fig. 7(b), the velocities of Zn^+ ions were estimated to be 1.4×10^4 and 9×10^3 m/s for the pairs of 170 and 270 ns and 270 and 370 ns, respectively. The fact that Zn^+ ions gradually decelerated in helium and had lower velocities than in vacuum

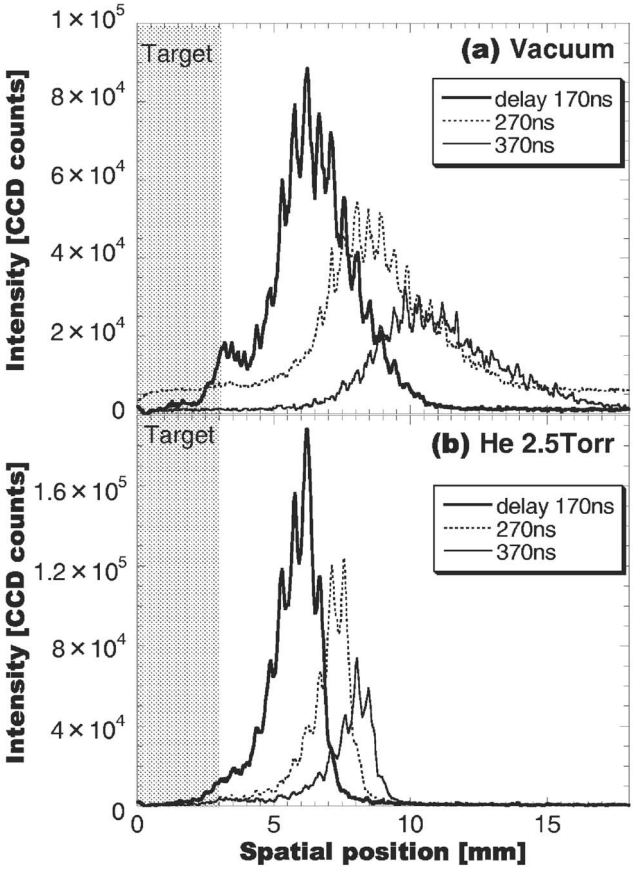

FIG. 7. Spatial distributions of the Zn^+ ion spectrum ($4D_{5/2}$-$4F_{7/2}$) at $t=170$, 270, and 370 ns in vacuum (a) and He at 2.5 Torr (b).

suggests that the particle expansion was suppressed by the collision with the ambient gas, as described later.

D. Recombination process in plasmas

1. Vacuum condition

Without the ambient gas, a plasma with a conical-shaped emission was generated. Figure 8 shows the time-integrated spatial distribution of the Zn atomic spectrum ($4\ ^3P_2$-$5\ ^3S_1$). The intense emission adjacent to the target was ascribed to the continuum emission at the initial stage. The emission

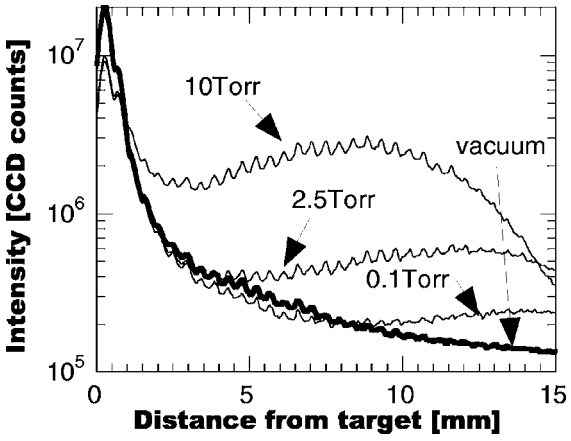

FIG. 8. Time-integrated spatial distributions of the Zn atom $4\ ^3P_2$-$5\ ^3S_1$ are shown for various He gas pressures.

intensity decreased monotonically along the normal to the target surface. The other atomic spectra exhibited similar distributions. Since the electrons and ions escape from the target faster than atoms, collisions between electrons and atoms do not take place frequently in vacuum. Moreover, if we assume that the plasma expansion is described by the hydrodynamic free expansion with an ideal flow and no viscosity, the thermal energy will be converted into a kinetic energy along the normal to the target surface. Thus, the collision frequency within the plume decreases due to the freezing of the perpendicular motion.[21] In addition, assuming that the electrons oscillate around the ion cloud, they could to some extent lose their energies via Coulomb collisions with ions. As a result, an expanding plasma with a low density and a moderate temperature is likely formed, in which the ions mainly recombine with electrons through the radiative recombination:

$$\mathrm{Zn}^+ + e \rightarrow \mathrm{Zn}(p) + h\nu. \tag{8}$$

It is of great significance to understand that electrons are preferably captured into the ground state or the lower excited p levels. Since the rate coefficient of reaction (8) is insensitive to the electron temperature, this process can take place even in slightly high-temperature plasmas. Indeed, Rydberg spectra originating from 3B recombination were not observed in vacuum (see below). Thus, the radiative recombination is believed to dominate the plasma neutralization in vacuum.

Meanwhile, the total amounts of the intensity given by spatial integration over the observation region for Zn^+ ions ($4\,^2D_{5/2}$-$4\,^2F_{7/2}$) and atoms ($4\,^3P_2$-$5\,^3S_1$) are shown in Figs. 9(a) and 9(b), respectively. In vacuum, the integrated intensity can be classified into two components defined by lifetimes, as shown in Fig. 9 with the solid curves. For Zn^+ ions, the intensity decreased rapidly with a time constant $\tau \sim 22$ ns during $t=150$ ns and thereafter decreased gently with $\tau \sim 330$ ns, whereas the radiative lifetime of the relevant transition ($\tau=6.3$ ns) was far shorter than the time scales over which emissions were observed. This clearly suggests that a mechanism for a population inflow into $4\,^2F_{7/2}$ was at play, followed by the radiative decay into the $4\,^2D_{5/2}$ level. Here, we note that at the initial stage, the population densities of the highly excited levels are expected to be high, since their distribution may be well described by LTE. Thus, it seems reasonable to suppose that the contribution of the cascades from upper levels into the $4\,^2F_{7/2}$ level via collisional and radiative decays can be predominant and can cause the emissions to be prolonged. At around $t=200$ ns, however, the dominant population inflow into $4\,^2F_{7/2}$ appears to change from cascading into radiative recombination, that is, $\mathrm{Zn}^{2+}+e \rightarrow \mathrm{Zn}^+(4\,^2F_{7/2})+h\nu$. A similar temporal behavior was obtained in atomic spectra, in which the long-lived emission may also be explained by the radiative recombination, i.e., $\mathrm{Zn}^+ + e \rightarrow \mathrm{Zn}(5\,^3S_1)+h\nu$, followed by the radiative decay $5\,^3S_1 \rightarrow 4\,^3P_2$.

2. Helium/oxygen atmospheres

A bright emission was observed in the He atmosphere, and the plasma size decreased with increasing gas pressure. For He pressures above 0.2 Torr, the emission region appeared spherical. The spatial distribution of the Zn atomic spectrum is shown in Fig. 8 for various He gas pressures. In contrast to the result observed in vacuum, the emission in helium had a well developed second maximum at a position far from the target.

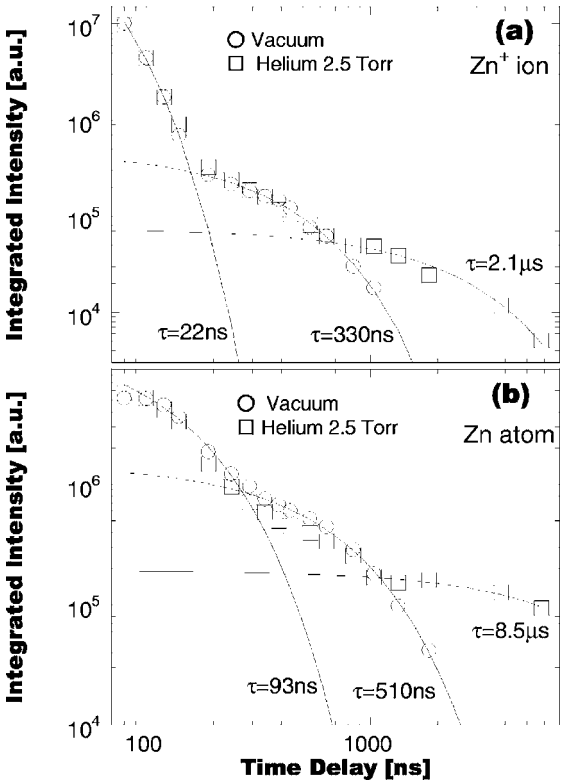

FIG. 9. Spatial-integrated intensity at different time delays in the Zn^+ ion $4D_{5/2}$-$4F_{7/2}$ (a) and the Zn atom $4\,^3P_2$-$5\,^3S_1$ (b). The best fitted exponential curves are represented by the solid curves.

The time-resolved spectra also revealed that at a delay t of 150 ns, the spatial distribution of the spectra in helium began to deviate from that in vacuum. As seen in Fig. 7(b), the emissions of the expansion front dropped dramatically, and the spectral intensity increased significantly compared with that in vacuum. This can be explained by the scattering and rapid cooling of the expanding plasma due to the contact with the ambient helium. That is, when the expanding plasma collides with the helium, the electrons, atoms, and ions within the plume depart from the initial trajectory, being also diffused along the lateral direction with respect to the target surface. As a result, the emission region appeared spherical in shape. Meanwhile, plasma electrons quickly lose their kinetic energy through elastic and inelastic collisions with helium, and consequently, a nonequilibrium plasma with a high density and a low temperature is presumably formed in the plume. Thus, the electrons recombine with ions through the 3B recombination, which is the dominant atomic process in high-density, low-temperature plasmas:[11,22]

$$\mathrm{Zn}^+ + e + M \rightarrow \mathrm{Zn}^*(p) + M, \tag{9}$$

where M represents a third body. The most important point of this recombination is that the electrons are captured into high Rydberg p levels and then collisionally deexcited into lower levels via ladderlike processes. Finally, the series of

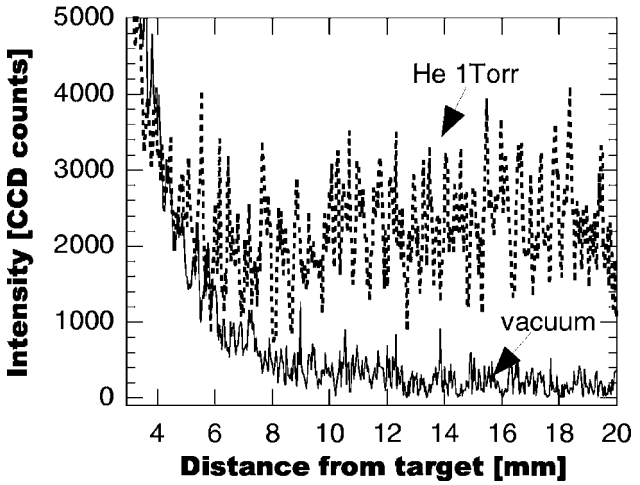

FIG. 10. Time-integrated spatial distributions of the Rydberg emission $4\,^1P$-$7\,^1S$ of the Zn atom in vacuum and He at 1.0 Torr. In the gas atmosphere, the Rydberg emission was observed at a great distance from the target.

recombination toward the ground state is terminated by an intense radiative decay. Consequently, the relaxation associated with the 3B recombination is longer than that in vacuum.

This is confirmed by the spatial integrated intensity (see Fig. 9). The temporal behavior of the Zn^+ intensity in helium was almost the same as that in vacuum, up to $t=700$ ns ($t=1000$ ns for atoms). After that, however, the intensity observed in helium was higher than that in vacuum. This temporal evolution clearly indicates that there exists an additional population mechanism into the Zn^+ ion $4\,^2F_{7/2}$ and the atom $5\,^3S_1$ levels in helium. Considering that the electrons are captured into highly excited levels, it seems reasonable that the cascade process via long-lived intermediate states gives rise to a slower decay of fluorescence in its tail. The reason why the peak intensity increased with the gas pressure and its position moved toward the target surface can also be ascribed to the 3B recombination, in which the expanding plasma undergoes a more efficient and rapid cooling with increasing pressure.

Further evidence of the 3B recombination is provided by the appearance of the emission associated with the Rydberg state. Figure 10 shows the time-integrated spatial distribution of the Zn atom $4\,^1P$-$7\,^1S$ in vacuum and He at 1 Torr. In helium, a Rydberg emission was observed at a great distance from the target, while no emission was observed in vacuum. A similar experiment using pure zinc also showed that the 3B recombination responsible for the intense emission played an important role in the plume.[23]

The bright emissions of Zn^+ ion spectra were also observed in helium, showing that the 3B recombination process, $Zn^{2+}+e+M \rightarrow Zn^{+*}(p)+M$, took place. This implies that the $Zn^{+*}(p)$ emission provides a signature of particles that was hitherto believed to be Zn^{2+} ions. However, the peak position of the Zn^+ ion spectrum appeared at a position closer to the target surface compared with that of the atom. A partial explanation for this observation can be derived from the fact that highly charged ions recombine with electrons sequentially and reduce their ionic stages in a stepwise manner, such as $Zn^{2+} \rightarrow Zn^+ \rightarrow Zn$ atom. Moreover, it should be noted that the recombination rate of Zn^{2+} ions is presumably more sensitive to temperature since the ionization potential of Zn^+ ions is higher ($I_p=17.96$ eV for the Zn ion; $I_p=9.39$ eV for the Zn atom).

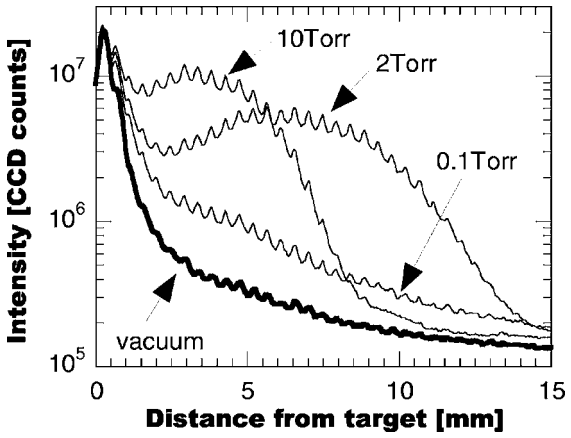

FIG. 11. Time-integrated spatial distributions of the Zn atom $4\,^3P_2$-$5\,^3S_1$ in oxygen as a function of gas pressure. Compared with the results in helium, much higher intensities whose peak positions appeared closer to the target were obtained.

For oxygen atmospheres, the peak position of the Zn atomic emission ($4\,^3P_2$-$5\,^3S_1$) also moved closer to the target with increasing pressure, as shown in Fig. 11. Compared with the results for the same gas pressure as that for helium, much more intense emissions were observed in the case of oxygen, while their peak positions shifted closer to the target surface than those in helium. It is reasonable to suppose that for oxygen, there are additional cooling processes, such as rotational and vibrational energy transfers. Figure 12 shows the time- and spatial-integrated spectra obtained under helium and oxygen at 1 Torr. The intensities of Zn ions in oxygen were ~7.2 times higher than those in helium, while the atomic Zn spectra in helium and oxygen differed by a factor of ~2.8. These results imply that the electrons cooled in oxygen may begin to recombine via the 3B recombination more rapidly compared to those cooled in helium. Consequently, the neutralization of plasmas which closely correlated with the deposition efficiency can be promoted in oxygen.

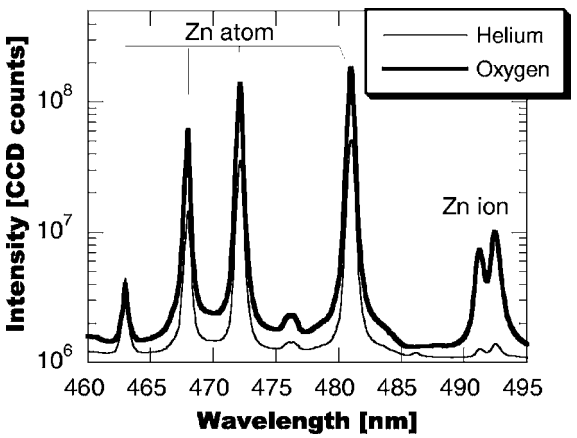

FIG. 12. Time- and spatial-integrated spectra of Zn ions and atoms in helium and oxygen under 1.0 Torr.

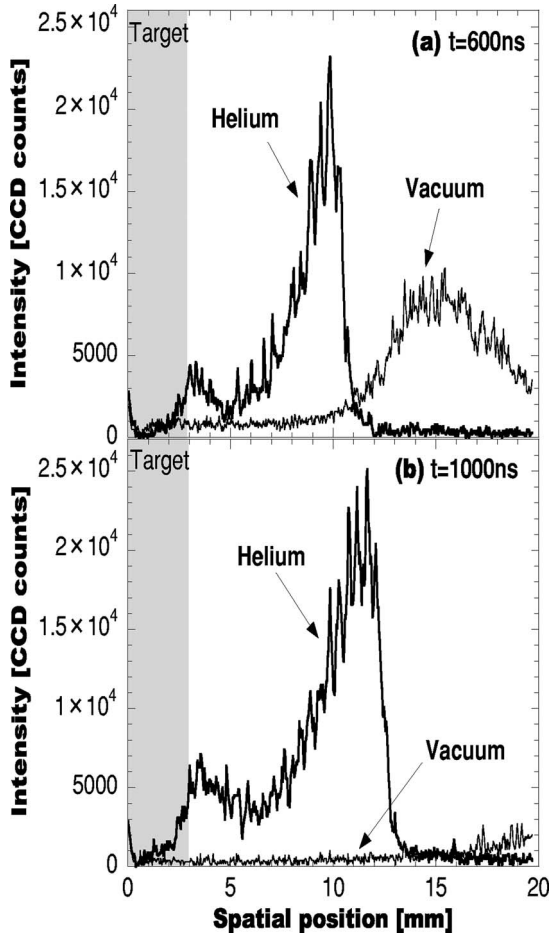

FIG. 13. Spatial distributions of the Zn^+ ion $4d\,^2D_{5/2}$-$4f\,^2F_{7/2}$ in vacuum and He at 2.5 Torr at a time delay of $t=600$ ns (a) and 1000 ns (b). It was found that in helium there appeared a small emission peak adjacent to the target well after the laser irradiation.

E. Charge exchange recombination in the He^+–Zn system

The spatial distributions of Zn^+ ionic spectra ($4\,^2D_{5/2}$ -$4\,^2F_{7/2}$) in vacuum and He at 2.5 Torr for the delays of (a) $t=600$ ns and (b) $t=1000$ ns are shown in Fig. 13. In vacuum, the emission region simply moved away from the target, while in helium, double peaks were observed. Although the second peak at around 10 mm moved slowly toward the right-hand side in Fig. 13(b), the position of the first peak remained constant throughout the measurements. This emission in the vicinity of the target cannot be explained by continuum spectra. One possible explanation may be the 3B recombination at an initial stage, during which the electrons may lose their energies rapidly via collisions with the ambient gas. However, since the electron and ion densities are still high enough at the initial stage, the plasma particles can to some extent penetrate through the ambient gas and not preferably remain adjacent to the target. Thus, it is reasonable to consider that recombination begins to occur around the second peak. In fact, since only the second peak of the Zn^+ ion emission was observed in oxygen, the phenomenon was inherent in helium.

The most probable origin of the first peak is to be found in the charge exchange process, followed by the collision with slow electrons:

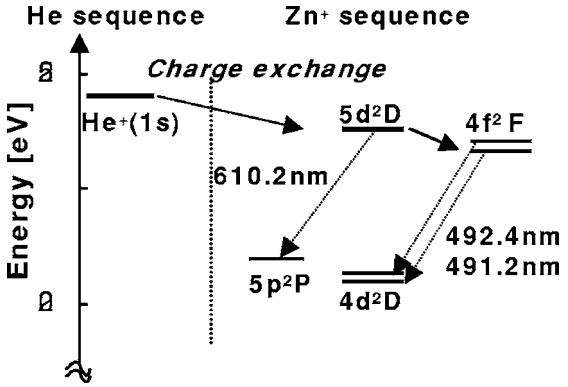

FIG. 14. The energy level diagram of He and Zn^+ ion sequences.

$$He^+ + Zn \rightarrow He(1s^2) + Zn^{+*}(5d\,^2D), \tag{10}$$

$$e + Zn^{+*}(5d\,^2D) \rightarrow e + Zn^{+*}(4f\,^2F). \tag{11}$$

These processes are well known as a mechanism of population inversion for the He–Zn blue laser.[24] The energy diagram of the He and Zn^+ sequences is shown in Fig. 14. In the present case, the electrons with high energies ionize He atoms at the initial stage. In fact, the intense emission of the He^+ ion transition ($n=4-6$) as well as the atomic spectra were observed only in the vicinity of the target. Considering that (i) the expansion of Zn atoms were suppressed in the gas atmosphere and (ii) He^+ ions did not have a velocity component in a specific direction, and their velocity may be given by the room temperature, it seems reasonable that near the target surface He^+ ions interact with Zn atoms through the processes expressed by Eq. (10), followed by the radiative decay from $4f\,^2F$.

IV. CONCLUSION

Spectroscopic investigations in laser-produced ZnO plasmas were carried out to study ablation and recombination dynamics on the basis of atomic physics. During and immediately after the laser irradiation, an intense continuum emission was observed near the target surface, which can be reproduced by the sum of the blackbody radiation from the target material and the thermodynamic equilibrium plasma.

The electron temperature and density were determined from the spectral profile and intensity of Zn atoms. The electron temperature deduced from the Boltzmann relationship of the excited levels was found to be several eV over 150 ns after the laser pulse. The electron density determined from the Stark broadening spectrum was $n_e \approx 3\times10^{25}$ m^{-3} at a delay of $t=40$ ns, while the electron density derived from the Stark shift was $n_e \approx 1\times10^{25}$ m^{-3}. This discrepancy can be explained by the fact that radiation trapping caused the intensity around the line center to drop significantly, resulting in the apparent broadened width. On the other hand, the expansion velocities of Zn ions and atoms in vacuum were determined by TOF to be $\sim 2\times10^4$ and $\sim 3\times10^3$ m/s, respectively. The remarkable difference in expansion velocity between the ions and atoms may provide evidence for an electric field leading to the acceleration of the charged particles.

As for the recombination process in vacuum, it was found that the radiative recombination was the dominant process in the plume. Meanwhile, under gas atmospheres, a long-lived bright emission that appeared spherical in shape was observed. Moreover, it was observed that the expansion of plasma particles was suppressed in gas atmospheres. This was ascribed to the scattering of ejected particles and the rapid plasma cooling due to the collision of electrons with the ambient gas, followed by the formation of low-temperature, high-density plasmas. Consequently, the 3B recombination responsible for the intense emissions dominated the plasma neutralization process. In addition, it was shown that oxygen may be effective for the rapid cooling and subsequent recombination.

Finally, the long-lived emission of the Zn^+ ions in the vicinity of the target was observed in helium, while in vacuum and oxygen atmosphere, this emission disappeared. This can be explained by the charge exchange process between the He^+ ions and Zn atoms.

ACKNOWLEDGMENT

This work is partly supported by the Grand-in-Aid for Young Scientists (B) (No. 17740366) from the Japan Society for the Promotion of Science and Electric Technology Research Foundation of Chugoku.

[1]Z. K. Tang, G. K. Wong, and P. Yu, Appl. Phys. Lett. **72**, 3270 (1998).
[2]Y. R. Ryu and T. S. Lee, Appl. Phys. Lett. **83**, 87 (2003).
[3]M. Makimura, T. Mizuta, and K. Murakami, Appl. Phys. A: Mater. Sci. Process. **69**, S213 (1999).
[4]M. Kawakami, A. B. Hartanto, Y. Nakata, and T. Okada, Jpn. J. Appl. Phys., Part 2 **42**, L33 (2003).
[5]D. B. Geohegan, Appl. Phys. Lett. **60**, 2732 (1992).
[6]N. Ohno, N. Ezumi, S. Takamura, S. I. Krasheninnkov, and A. Yu, Phys. Rev. Lett. **81**, 818 (1998).
[7]B. H. Bransden and C. J. Joachain, *Physics of Atoms and Molecules* (Longman Scientific & Technical, New York, 1983).
[8]F. Claeyssens, A. Cheesman, S. J. Hnley, and M. N. Ashfold, J. Appl. Phys. **92**, 6886 (2002).
[9]R. W. P. McWhirter, in *Plasma Diagnostic Techniques*, edited by R. H. Huddlestone and S. L. Leonard (Academic, New York, 1965).
[10]M. Otsuka, R. Ikee, and K. Ishii, J. Quant. Spectrosc. Radiat. Transf. **21**, 41 (1979).
[11]S. Namba, M. Goto, H. Tsuboi, T. Oda, and K. Sato, J. Appl. Phys. **88**, 3182 (2000).
[12]H. R. Griem, *Plasma Spectroscopy* (McGraw-Hill, New York, 1964).
[13]H. R. Griem, *Spectral Line Broadening by Plasmas* (Academic, New York, 1974).
[14]N. Konjevic, Phys. Rep. **316**, 339 (1999).
[15]G. Traving, in *Plasma Diagnostics*, edited by W. Lochte-Holtgreven (North-Holland, Amsterdam, 1968).
[16]A. Unsöld, *Physik der Sternatmosphären* (Springer, Berlin, 1968).
[17]M. Born, J. Phys. D **32**, 2492 (1999) and references therein.
[18]C. Girault, D. Damiani, J. Aubreton, and Y. Nishina, Appl. Phys. Lett. **54**, 2716 (1989).
[19]J. F. Ready, *Effects of High Power Laser Radiation* (Academic, New York, 1971).
[20]T. P. Hughes, *Plasma and Laser Light* (Hilger, London, 1975).
[21]D. R. Miller, in *Atomic and Molecular Beam Methods*, edited by G. Scoles (Oxford University Press, New York, 1988), Vol. 1.
[22]H. Akatsuka and M. Suzuki, Contrib. Plasma Phys. **34**, 539 (1994).
[23]S. Gogić and S. Milošević, Fiz. A **7**, 37 (1998).
[24]M. Jánossy and P. Mezei, Appl. Phys. B: Lasers Opt. **66**, 47 (1998).